Evolution of the ELOCA Code: Mk6 to the Present

V.I. Arimescu, M.E. Klein, J.R. Gauld,

Z.W. Lian and L.N. Carlucci

AECL Research Chalk River Laboratories Chalk River, Ontario, K0J 1J0

1. Introduction

Knowledge of fuel element behaviour during off-normal and accidental reactor transients is important for the safety and licensing of CANDU reactors. In transients such as a large break loss-of-coolant accident (LOCA), fuel and sheath temperatures increase rapidly due to impaired heat transfer to the coolant, coupled with a large power peak. This will result in an increase in internal gas pressure and a decrease in the sheath strength. Ballooning deformation of the sheath will occur once the coolant pressure drops below the element internal gas pressure, with the potential for sheath failure and subsequent release of fission products into the reactor cooling system.

ELOCA is a computer code developed to model the thermo-mechanical response and associated fission gas release (FGR) behaviour of CANDU fuel elements during high-temperature LOCA-type transients. The latest version, ELOCA.Mk6 is capable of performing an axisymmetric analysis of a CANDU fuel element, accounting for axial variations in sheath temperatures, metallurgical variables and reactor neutron flux. ELOCA.Mk6 couples thermo-mechanical analysis with calculations for the formation, diffusion, sweeping, swelling and release of gaseous fission products from the fuel.

ELOCA.Mk6

ELOCA.Mk6 is the latest version of a series of ELOCA codes [1], that combines axial segmentation with an improved pellet-to-sheath mechanical contact model [2]. Also, ELOCA.Mk6 integrates the FREEDOM [3] gaseous fission-product release model with the fuel-element thermo-mechanical response. This integration allows for feedback mechanisms between gaseous fission-product release and swelling, and the thermo-mechanical response, thereby providing a more realistic modelling of overall fuel element behaviour.

ELOCA.Mk6 accounts for the following thermo-mechanical and gaseous fission product release (FGR) phenomena:

- Expansion, contraction, cracking, and melting of the fuel,
- Variations in the element internal gas pressure,
- Changes in the fuel-to-sheath heat transfer,
- Deformation of the sheath,
- Zr/H₂O chemical reaction,
- Beryllium-assisted cracking of the sheath,
- Fission gas formation and loss by decay and neutron capture,
- Grain growth,
- Fission gas diffusion,
- Grain boundary sweeping of fission gases,
- Fission gas release by bubble growth and grain face separation, and
- Fission gas swelling.

ELOCA.Mk6 extends the capability of ELOCA to model element behaviour after sheath failure [4]. The post-failure phenomena included are:

- Element depressurization upon sheath failure,
- Changes in gap conditions due to steam ingress,
- Fission gas transport along the fuel-to-sheath gap and release to the coolant at the failure location, and
- Behaviour of a pre-defected element under LOCA conditions.

Other new features and improvements include:

- Optional sheath oxide-strengthening based on the TOSS model [5],
- Sheath failure due to oxygen embrittlement,
- Effect of pellet-bottoming on fuel-to-sheath heat transfer,
- Improved ELESIM-ELOCA interface,
- Option to calculate release of user-specified gaseous isotopes,
- Improved speed and robustness,
- Capability to run on VAX/VMS, APOLLO/UNIX, HP/UNIX, IBM-RISC/UNIX and PC systems, and
- Consistent internal documentation for each module,

ELOCA.Mk6 also allows a fuel element to be subdivided into a maximum of 20 axial segments. Segmentation is used to account for axial variations in thermalhydraulic conditions, element power, Zircaloy microstructure, fuel physical state, fuel-to-sheath heat transfer, and sheath oxidation and deformation. The axial segments are connected through a mechanical contact model, while the heat conduction equation is solved independently for each axial segment. The internal gas pressure assumes rapid pressure equilibration and thermodynamic equilibrium which allows the ideal gas law to be used to calculate the overall element gas pressure from the moles of gas at different temperatures in the free volumes of all the segments.

Fuel and sheath temperatures are calculated using a semi-implicit (Crank-Nicholson type) finite-difference method where the fuel element is subdivided into a maximum of 100 concentric radial annuli. The method accounts for radial conduction (assuming axial symmetry) of heat through the fuel element (composed of UO₂ pellet, radial pellet-to-sheath gap and sheath), and includes heat generation from the Zircaloy/steam chemical reaction and the effects of latent heat of Zircaloy phase change and UO₂ melting. The sheath-to-coolant heat transfer coefficient is an input to the code and comes from a thermal-hydraulic code (as discussed below, ELOCA can be coupled with a thermal-hydraulic code can be done within an integrated code system). As well, the heat generation rate is supplied as an input by a dynamic reactor-physics code.

The pellet-to-sheath mechanical contact model calculates the stresses generated when straining is imposed by mechanical contact between fuel pellet and sheath, either radially, axially, or both directions simultaneously. When there is no mechanical ontact, the strain rate is calculated based on stresses determined by the internal gas pressure and the outside coolant pressure (which is the second input required of a thermal-hydraulic code) and derived according to the thin membrane model.

The sheath plastic deformation model uses a strain-rate constitutive equation. It is a microstructurally based model that includes the effects of grain size, recrystallization, phase change and hardening/recovery on the creep rate [6]. The latter processes are represented in the model by an internal stress parameter.

Sheath oxide-strengthening and the effect of pellet bottoming (eccentricity) on fuel-to-sheath heat transfer were two of the new features implemented in ELOCA.Mk6. They are discussed further below.

3. New ELOCA.Mk6 Features

The models for sheath oxide-strengthening and pellet bottoming are briefly described and simulation results presented for demonstration purposes.

Sheath Oxide-Strengthening

The sheath oxide-strengthening model implemented in ELOCA.MK6 is based on the work of Sagat et al. [5]. It can be divided into three separate components. The first component deals with uncracked oxide and allows for a reduction of the stress in the substrate by the amount of the applied stress that may be supported by the intact oxide layer. The second component describes the opening of cracks in the oxide layer and the development of their geometry, as well as their contribution to the total creep strain. The third component covers the strengthening effect of dissolved oxygen in the α -Zr layer through the use of an empirical correction factor.

Uncracked Oxide

The first component of the model, describing the load supporting ability of the uncracked oxide layer, is based on the assumption that this layer is made up of a purely elastic material.

Upon formation of the oxide layer, a compressive strain is introduced in the oxide layer, known as the "formation strain", ϵ_f . This is due to the lower oxide density, which results in a volume expansion of the oxide layer.

The stress applied to the oxide layer is then given by:

$$\sigma_0 = E(\varepsilon_0 - \varepsilon_f) \tag{1}$$

where

 ε_0 = average strain across the oxide due to substrate deformation,

E = Young's Modulus.

A force balance across the sheath cross-section yields the stress applied to the metal substrate layer as:

$$\sigma_{\theta} = \sigma_{\theta app} \frac{W_o + W_m}{W_m} - \sigma_0 \frac{W_o}{W_m}$$
(2)

where

W_o = thickness of the oxide layer,

 W_m = thickness of the metal substrate,

 $\sigma_{\theta ann}$ = applied hoop stress due to external load.

If $\sigma_{\theta app}$ and σ_{θ} are of opposite signs, then the oxide layer supports the applied stress and creep will not occur. In this case, the creep strain rate is set to zero.

If, however, these two stresses act in the same direction, then the strain rate is calculated such that both the oxygen-rich α -Zr layer and the metal substrate layer are subjected to the same strain rate. This calculation is performed numerically with the creep rate of the α -Zr layer being corrected for strengthening due to increased oxygen concentration, as described below. The procedure consists of iteratively splitting the applied stress, as given by Equation (2), into two components until the two creep strain-rates are equal within a convergence limit.

Oxide Cracks and Resulting Sheath Deformation

Oxide cracking is deemed to start with a single crack when the average strain imposed on the oxide layer exceeds 1.8% and to reoccur by doubling the number of cracks with every additional 0.5% average strain. A maximum number of 12 families of cracks is allowed based on experimental data [5].

If a crack has just opened, then an initial crack width of zero is assigned. The depth of the crack is a function of sheath temperature. For temperatures less than 1083 K (temperature at which the alpha to beta phase change begins), the crack depth is assumed to be zero. For higher temperatures, the crack depth, d_{crack} , is defined as a function of the α -Zr layer thickness and is proportional to the oxygen penetration, which leads to the following relation:

$$d_{crack} = 1.2 \sqrt{D_{\alpha ZR}} \frac{W_{\alpha Zr}}{C_{\alpha Zr}}$$
(3)

where

 $D_{\alpha Z_f}$ = diffusion coefficient of oxygen in the α -Zr layer,

 $W_{\alpha Z_r}$ = thickness of α -Zr layer,

 $C_{\alpha Zr}$ = parabolic rate constant for the growth of the α -Zr layer.

For existing cracks, a number of crack parameters under the crack tip are defined, including gauge length, l_g and stress, $\sigma_{\theta c}$:

$$l_g = (W_{Zrc} + W_{\alpha Zrc}) \exp(-\varepsilon_{0c})$$
(4)

$$\sigma_{\alpha} = \sigma_{\theta} W_m \frac{\exp(-\varepsilon_{0c})}{l_g} \tag{5}$$

where

W_{Zrc} = thickness of metal substrate under the crack tip,

 $W_{\alpha Zrc}$ =thickness of α -Zr under the crack tip,

 ε_{0c} = strain under the crack tip, estimated from the previous time step.

The thickness of the beta-Zr substrate (excluding the α -Zr layer) under the crack tip is diminished by the growth of the α -Zr layer, while the crack width expands according to:

$$dw/dt = 2l_g(d \varepsilon_c/dt - d \varepsilon_{loc}/dt)$$
(6)

In the above relation, ε_c is the strain at the tip of the crack, calculated using the stress given by equation (5).

Finally, the contributions of all crack widths are summed with the contribution of the strain away from the cracks to obtain an average sheath strain to be used in further calculations by the code.

Strengthening Effect of Dissolved Oxygen

It is known that oxygen dissolves in the Zircaloy matrix as an interstitial and has a strengthening effect on its deformation[5]. This effect must be considered for the oxygen-rich α -Zr layer that forms underneath the oxide layer.

The following empirical correlation has been derived from experimental data, to describe the correction factor on the α -Zr creep, which depends on C[wt %], the local oxygen concentration [5]:

$$k(C) = e^{-3.42(C-0.126)} + 0.1e^{-2.19C}$$
(7)

Since, the oxygen concentration varies in the α -Zr layer, the global effect is calculated as the integrated average, assuming that creep is uniform throughout the α -Zr layer and that the total load is distributed to satisfy this condition of uniform creep. Using a stress exponent of 5.3 for the creep of α -Zr the following relation can be derived for the average correction factor, to be applied to the α -Zr layer as a whole:

$$K = \left(\int \frac{1}{k^{1/5.3}} \, dx \right)^{-5.3} \tag{8}$$

Figure 1 shows results from a simulation of the CANDU/PBF[7] test using the oxide strengthening capability implemented in ELOCA.Mk6. Calculated plastic hoop strains, with and without oxide strengthening, are compared to the measured values. The calculated plastic hoop strains underpredict the measured strain in the upper-half of the element and overpredict the measured strain in the lower-half. However, use of the oxide-strengthening option results in a strain profile that better captures the shape of the measured profile. The average strain calculated with the oxide-strengthening option is in good agreement with the average measured strain (10.7% versus 11.8%).

Effect of Pellet Bottoming

Pellet eccentricity (commonly called pellet bottoming) affects the fuel-to-sheath heat transfer, which in turn changes the thermal-mechanical response of the fuel element and the fission gas release. A model was implemented in ELOCA.Mk6 that calculates the effective fuel-to-sheath heat transfer coefficient under pellet-bottoming conditions.

The model accounts for the eccentricity by including the local gap width in the local gap conductance calculation for any angle:

$$h_g(\theta) = \frac{k_g}{C_r + C_c + C_t + d(1 - \cos \theta)}$$
(9)

where:

k_g - gas thermal conductivity

C_r - accounts for fuel and sheath roughness

C_c - accounts for the CANLUB effect

C, - temperature jump distance

d - $r_s - r_f$ (r_f is the pellet radius and r_s is the sheath inner radius)

For a fully eccentric case, the eccentricity offset will equal d.

The effective gap conductance is defined as a circumferentially averaged value and is calculated as:

$$\frac{\overline{h}_{g}}{\overline{h}_{g}} = \frac{1}{2\pi} \int_{0}^{2\pi} \overline{h}_{g}(\theta) d\theta$$

$$= \frac{h_{n}}{\sqrt{1 - \left(\frac{d}{C_{r} + C_{c} + C_{1} + d}\right)^{2}}}$$

$$= f_{ecc} \times h_{n}$$
(10)

where f_{ecc} is the eccentricity factor:

$$f_{ecc} = \frac{1}{\sqrt{1 - \left(\frac{d}{C_r + C_c + C_t + d}\right)^2}}$$
 (11)

and h_n is the nominal gap conductance calculated for a concentric pellet and cladding:

$$h_{n} = \frac{k_{g}}{C_{c} + C_{c} + C_{c} + d}$$
 (12)

The results of a test run with for pellet-bottoming are compared with that of a reference case (concentric pellet) in Figures 2 to 5. Starting from t = 900 s when a fuel-to-sheath gap is formed, a higher fuel-to-sheath heat transfer coefficient and a lower fuel temperature are observed for the pellet-bottoming case (Figures 2, 3). The lower fuel temperature, in turn, results in less fission gas release (Figure 4) which contributes to a lower gas pressure in the gap, and finally, to a lower sheath strain.

4. ELOCA.Mk6 Development

4.1 Subroutine Version of ELOCA.Mk6

A subroutine version, ELOCA.Mk6 Mod1, was developed from ELOCA.Mk6 Mod0 for use as the fuel model with thermalhydraulics codes such as ASSERT or CATHENA. As a result, the feedback between various phenomena and processes in a fuel channel can be better modelled. A series of interface modules were developed to coordinate the mapping and transfer of information between the separate codes. The temperature solver in Mk6 Mod1 was supplemented by a two-dimensional (2-D) finite control volume (FCV) temperature solver, TEMDRIV, as required for the 2-D treatment of the radiative heat transfer in a channel.

Interface

The approach taken to coupling ELOCA.Mk6 to thermalhydraulics codes as a subroutine required minimal changes to both codes while allowing flexibility for application to other code systems. The result was a code coupling architecture involving several interface routines. Interface routines were written in FORTRAN-77 to allocate memory for multiple ELOCA applications, to process thermalhydraulic boundary conditions from a given thermalhydraulics code, and to feed back the calculated temperature, geometry, and other desired output parameters from ELOCA. The overall structure of the interface is flexible enough to accommodate different modes of operation and new features resulting from the future development of the

component codes, with minor effort. When used as a subroutine, the specification of the ELOCA input is handled by the thermalhydraulics code.

A driver program was written for the ELOCA interface to allow the subroutine version of ELOCA to be used as a standalone program.

Two-Dimensional Temperature Solver

The 2-D FCV temperature solver, TEMDRIV, allows the circumferential variations in fuel temperature to be calculated. It uses an alternating direction implicit (ADI) solver to solve the FCV equations and has modifications for improved convergence and robustness (i.e., implicit over-relaxation of temperature). TEMDRIV also includes models for the following phenomena: material properties for UO₂, Zr, ZrO₂, and Graphite; latent heat effects due to phases change; pellet bottoming; latent heat effects due to UO₂ melting; and heat generation in the sheath from the metal/water reaction.

4.2. Other Recent Developments

Additional ELOCA.Mk6 development has focused on enhancing its fission gas release capability through segmentation of the FREEDOM model and by modelling FGR in oxidizing environments.

Segmentation

Currently, as for its thermo-mechanical calculations, ELOCA can perform a FGR simulation for up to twenty axial segments. The FREEDOM FGR model has been extended to handle axial segments allowing the effects of axial variations in fuel power and geometry on FGR to be modelled.

Fission Product Release in an Oxidizing Environment

Additional development work in the FGR area has been concerned with implementing in ELOCA the capability to model fission gas release in an oxidizing environment. To this end, the Turnbull et al. model [8] of the effect of hyperstoichiometry of UO₂ on the diffusion coefficient of fission products has been implemented, with a UO₂ oxidation model from experimental measurements made at AECL [9]. The latter model is applied to each annulus in the pellet independently. Further work will provide a model for coupling between the pellet annuli to account for oxygen diffusion in the concentration and thermal gradients existing across the pellet.

6. Conclusions

ELOCA is a full-featured fuel code that has been continuously improved through the development and implementation of new features as presented here.

Further improvements being considered for ELOCA include upgrades of the FROM.SFD oxidation module, and replacing the FREEDOM numerical solution with an analytical solution. Nevertheless, the emphasis in the near future will be on validation of ELOCA.Mk6 according to a rigorous and formal methodology, known as the Validation Matrix Methodology.

7. References

- [1] H.E. Sills, "ELOCA Fuel Element Behaviour during LOCA," AECL Report, AECL-6357, 1980.
- [2] V.I. Arimescu, "An Elasto-Plastic Model for Mechanical Contact Between the Pellets and Sheath in CANDU Nuclear Fuel Elements," AECL Report AECL-10426, 1991.

- [3] L.D. MacDonald, D.B. Duncan, B.J. Lewis and F.C. Iglesias, "FREEDOM: A Transient Fission-Product Release Model for Radioactive and Stable Species", AECL Report AECL-9810, 1988.
- [4] Z.W. Lian, L.N. Carlucci, and V.I. Arimescu, "Convective-Diffusive Transport of Fission Products in the Gap of a Failed Fuel Element," AECL Report AECL-11134, 1994.
- [5] S. Sagat, H.E. Sills and J.A. Walsworth, "Deformation and Failure of Zircaloy Fuel Sheaths under LOCA Conditions", AECL Report AECL-7754.
- [6] H.E. Sills and R.A. Holt, "NIRVANA, A High Temperature Creep Model for Zircaloy Fuel Sheaths", AECL Report AECL-6412, 1979.
- [7] E. Kohn, P.J. Fehrenbach and J.H.K. Lau, "CANDU Fuel Behaviour Under LOCA Conditions," AECL Report, AECL-9788, April 1989
- [8] J.C. Killeen and J.A. Turnbull, "An Experimental and Theoretical Treatment of the Release of Kr85 from Hyperstoichiometric Uranium Dioxide", Workshop on Chemical Reactivity of Oxide Fuel and Fission Product Release, April 7-9, 1987
- [9] D.S. Cox, Z. Liu, P.H. Elder, C.E.L. Hunt, and V.I. Arimescu, "Fission Product Release Kinetics from CANDU and LWR Fuel During High-Temperature Steam Oxidation Experiments", Technical Committee Meeting, Pembroke 1992, IAEA-TECDOC-697, April 1993.

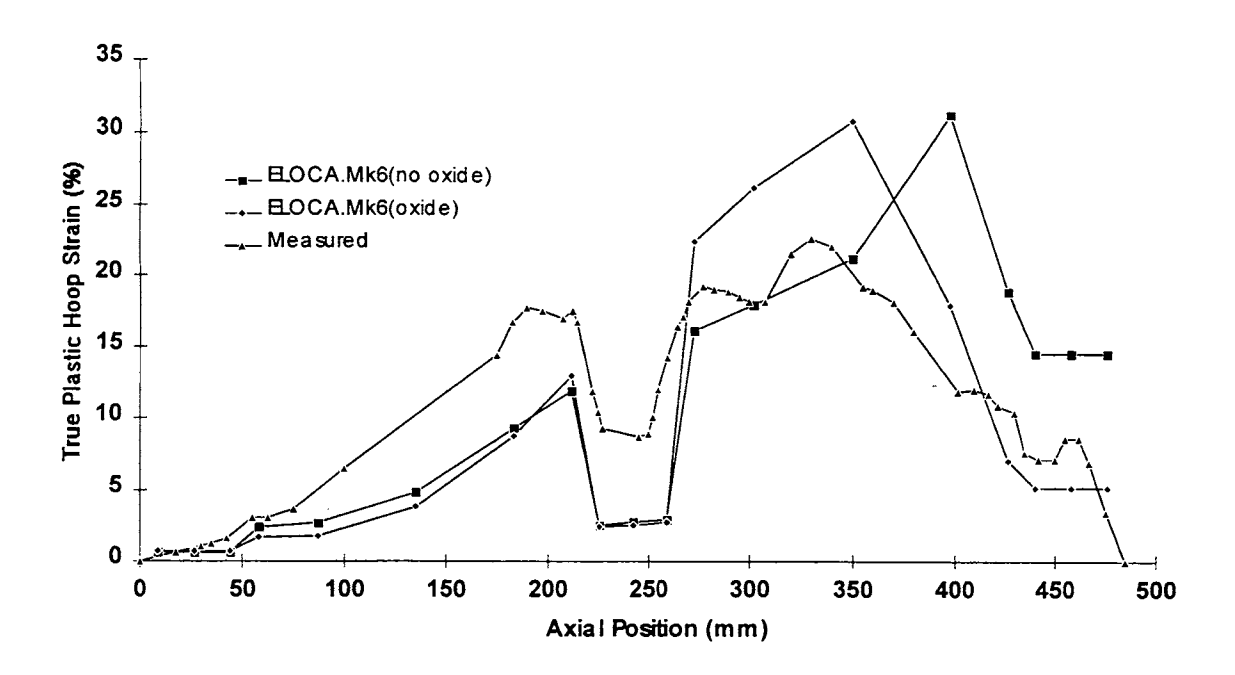


Figure 1: Comparison of ELOCA.Mk6 Calculated Plastic Hoop Strain (with and without oxide strengthening) with Measured Values for CANDU/PBF

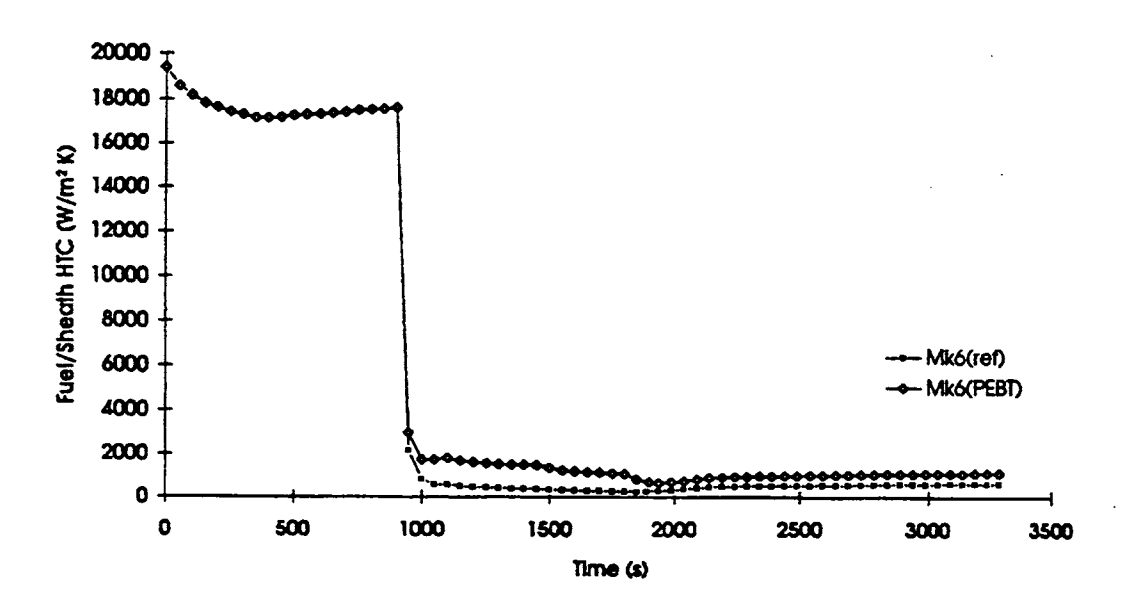


Figure 2: Comparison of Fuel-to-Sheath Heat Transfer Coefficients under Pellet Bottoming and Concentric Conditions

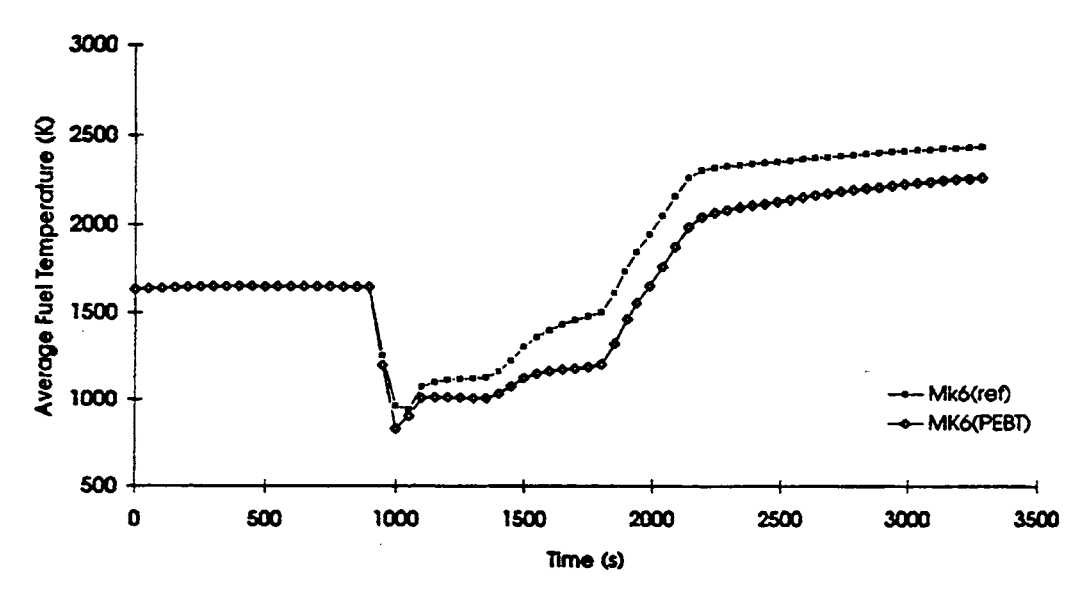


Figure 3: Comparison of Average Fuel Temperatures under Pellet Bottoming and Concentric Conditions

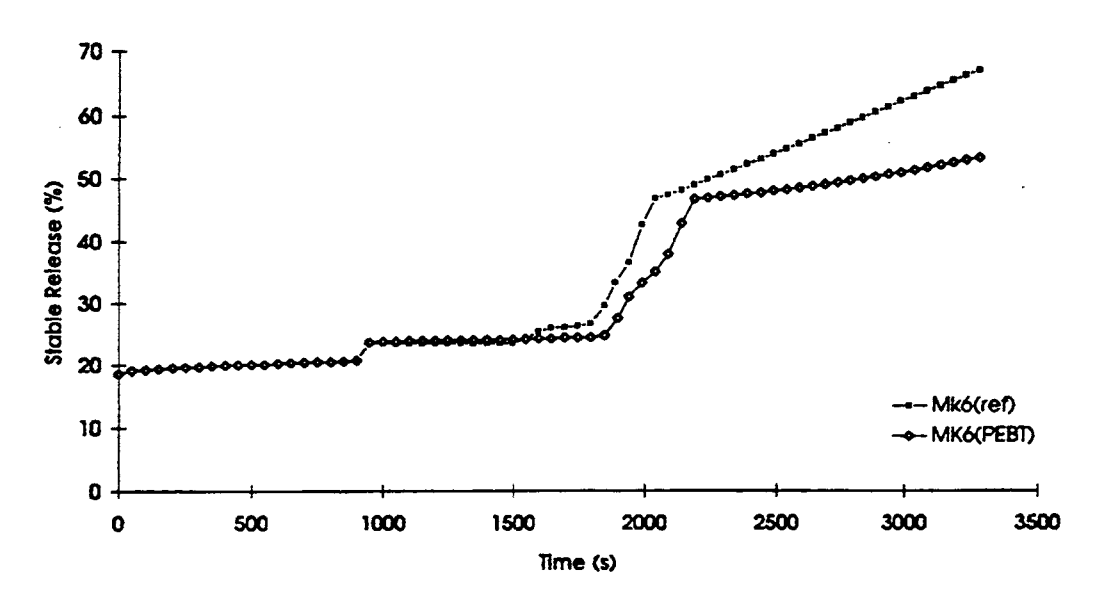


Figure 4: Comparison of Stable Gas Releases to the Gap under Pellet Bottoming and Concentric Conditions